



# Development and testing of a novel sulfur dioxide sonde

Subin Yoon<sup>1</sup>, Alexander Kotsakis<sup>1,a</sup>, Sergio L. Alvarez<sup>1</sup>, Mark G. Spychala<sup>2,b</sup>, Elizabeth Klovenski<sup>1</sup>, Paul Walter<sup>2</sup>, Gary Morris<sup>2,c</sup>, Ernesto Corrales<sup>3</sup>, Alfredo Alan<sup>3</sup>, Jorge A. Diaz<sup>3,d</sup>, and James H. Flynn<sup>1</sup>

<sup>1</sup>Department of Earth and Atmospheric Sciences, University of Houston, Houston, TX, 77004, USA

<sup>2</sup>School of Natural Sciences, St. Edward's University, Austin, TX, 78704, USA

<sup>3</sup>GasLAB, CICANUM, Universidad de Costa Rica, San José, Costa Rica

<sup>a</sup>now at: ERT, Inc., Laurel, MD, 20707, USA

<sup>b</sup>now at: Hamelmann Communications, Pagosa Springs, CO, 81147, USA

<sup>c</sup>now at: NOAA Global Monitoring Laboratory, Boulder, CO, 80305, USA

<sup>d</sup>now at: INFICON, East Syracuse, NY, 13057, USA

**Correspondence:** James H. Flynn (jhflynn@central.uh.edu)

Received: 26 February 2022 – Discussion started: 3 March 2022

Revised: 7 June 2022 – Accepted: 13 June 2022 – Published: 29 July 2022

**Abstract.** A novel technique has been developed to measure sulfur dioxide (SO<sub>2</sub>) using a modification of the existing electrochemical concentration cell (ECC) ozonesonde technology. The current sonde-based method to measure SO<sub>2</sub> (i.e., the dual-sonde approach) involves launching two ozonesondes together, with one of the sondes having a filter to remove SO<sub>2</sub> at the inlet. The SO<sub>2</sub> profile is determined by taking the difference between the measurements from the two instruments. The dual-sonde method works well in typical tropospheric conditions when [O<sub>3</sub>] > [SO<sub>2</sub>] but saturates when [SO<sub>2</sub>] > [O<sub>3</sub>] and has large uncertainties in the upper troposphere and lower stratosphere that would limit its effectiveness in measuring SO<sub>2</sub> from an explosive volcanic eruption. Due to these limitations, several modifications were made to create a single-sonde system that would directly measure SO<sub>2</sub> (i.e., the SO<sub>2</sub> sonde). These modifications included (1) a positively biased ECC current, (2) the addition of an O<sub>3</sub> removal filter, and (3) the addition of a sample dryer. The SO<sub>2</sub> sonde measures SO<sub>2</sub> as a reduction in the cell current. There was a strong correlation ( $r^2 > 0.94$ ) between the SO<sub>2</sub> sonde and a Thermo 43c analyzer during controlled laboratory tests and pre-flight tests. Varying humidity levels affected the SO<sub>2</sub> sonde's sensitivity ( $\text{avg} = 84.6 \pm 31.7 \text{ ppbv } \mu\text{A}^{-1}$ ,  $1\sigma \text{ RSD} = 37\%$ ) during initial field tests, which was resolved by adding a sample dryer upstream of the O<sub>3</sub> removal filter and pump inlet. This modification significantly reduced the variability and increased the sensitivity of the SO<sub>2</sub> measurements ( $\text{avg} = 47 \pm 5.8 \text{ ppbv } \mu\text{A}^{-1}$ ,

$1\sigma \text{ RSD} = 12\%$ ). Field tests included measurements near Kilauea volcano (before and during the 2018 eruption of the Lower East Rift Zone), Costa Rica's Turrialba volcano, and anthropogenic plumes from the Athabasca oil sands region of Alberta, Canada. This single-SO<sub>2</sub>-sonde system is an effective, inexpensive instrument for measuring both ground-based and vertical profiles of SO<sub>2</sub> from anthropogenic and natural sources (i.e., volcanic eruptions) over a wide range of concentrations.

## 1 Introduction

Sulfur dioxide (SO<sub>2</sub>) emissions result from anthropogenic activities, such as power generation and crude oil refining processes, and natural sources, such as volcanoes. In gas form, SO<sub>2</sub> acts as a respiratory irritant, leading to complications with asthma and cardiovascular conditions (Chen et al., 2007; Sunyer et al., 2003; Tzortziou et al., 2015, 2018). Gaseous SO<sub>2</sub> can be converted to sulfate aerosols (Zhang et al., 2015), which are highly scattering, reduce visibility, and can have a cooling effect on the surface climate when injected into the stratosphere (Kiehl and Briegleb, 1993; Schmidt et al., 2010). SO<sub>2</sub> acidifies rain, accelerating damage of infrastructure and vegetation, particularly near SO<sub>2</sub> sources such as volcanoes (Delmelle et al., 2002; Krug and Frink, 1983; Tortini et al., 2017). Due to these various climate, environmental, and human health-related im-

pacts, anthropogenic SO<sub>2</sub> has been heavily monitored (Shannon, 1999; Zhang and Schreifels, 2011), and regulations have been enacted to reduce these emissions (EPA, 2000).

The largest natural sources of SO<sub>2</sub> are volcanoes. The eruption of Mt. Pinatubo in the Philippines in June 1991 had global climatic effects and significant impacts on the tropospheric and lower stratospheric composition (Bluth et al., 1992; Parker et al., 1996). Apart from such catastrophic eruptions, SO<sub>2</sub> can be continually emitted from volcanoes. SO<sub>2</sub> plumes from over 90 volcanoes have been reliably detected by satellites, resulting in the injection of an estimated  $23 \pm 2 \text{ Tg yr}^{-1}$  of SO<sub>2</sub> into the atmosphere (Carn et al., 2017). However, unlike anthropogenic sources of SO<sub>2</sub>, most volcanoes lack routine ground monitoring (Galle et al., 2010; Pieri et al., 2013), and few opportunities exist for routine validation of satellite retrievals of SO<sub>2</sub> with in situ measurements. Small unmanned aerial vehicle (UAV) platforms can measure volcanic plumes at altitudes of 2 km above the take-off altitude (Galle et al., 2010; Diaz et al., 2015) while larger UAVs can measure stratospheric plumes (e.g., Global Hawk). However, the lack and difficulty of monitoring and the possibility of another stratospheric injection of SO<sub>2</sub> motivated the development of an inexpensive but reliable balloon-borne instrument that could be deployed quickly after an eruption to validate satellite observations with in situ measurements.

Radiosondes and ozonesondes have been widely used for measurements of various atmospheric parameters (e.g., temperature, air pressure, relative humidity (RH), wind speed and direction, and O<sub>3</sub> concentrations). Electrochemical concentration cell (ECC) ozonesondes produce vertical O<sub>3</sub> profiles and allow for the validation of satellite-based O<sub>3</sub> vertical column density (VCD). A schematic of the ECC is included in Fig. S1 in the Supplement. The current sonde-based method for measuring SO<sub>2</sub>, the dual-sonde method, uses two En-Sci (Environmental Science Inc., Westminster, CO) ECC ozonesondes in tandem (Morris et al., 2010). For the dual-sonde method, an SO<sub>2</sub> removal filter is placed at the pump inlet of one of the ozonesondes, scrubbing SO<sub>2</sub> from the sampled air before it enters the ECC. The other sonde samples unfiltered air (i.e., air containing both SO<sub>2</sub> and O<sub>3</sub>). Due to the chemical reactions in the cathode cell, the filtered sonde measures O<sub>3</sub>, while the unfiltered sonde measures the difference between O<sub>3</sub> and SO<sub>2</sub> ( $[\text{O}_3] - [\text{SO}_2]$ ) since SO<sub>2</sub> has an equal (relative to O<sub>3</sub>) but negative signal in the ECC (Morris et al., 2010). The SO<sub>2</sub> concentrations are then determined from the difference between the two sonde measurements. This method works well in the troposphere when the SO<sub>2</sub> concentration is less than the O<sub>3</sub> concentration, but not as well in intense plumes, such as those found in eruptive volcanic environments. When the SO<sub>2</sub> concentration exceeds the O<sub>3</sub> concentration, the cell current in the unfiltered sonde becomes zero. The excess SO<sub>2</sub> saturates the dual sonde and distorts the calculated SO<sub>2</sub> profile. Additionally, in the stratosphere, where the O<sub>3</sub> signal grows much larger than in the troposphere, the combined uncertainty of the measurements

of the filtered and unfiltered sondes results in a large lower limit of detection (LLOD), on the order of tens of parts per billion by volume. Thus, a field deployment of the dual-sonde method more than a few days after an explosive, tropical volcanic eruption such as Mt. Pinatubo would result in few useful data in the critical upper troposphere–lower stratosphere region.

This study reports on the development of a single instrument capable of in situ SO<sub>2</sub> measurements in the presence or absence of O<sub>3</sub>. This sonde can measure SO<sub>2</sub> at much greater concentrations than O<sub>3</sub> without saturating the system and can be configured for a sub-ppbv LLOD (calculated using  $3\sigma$ ) at sea level. Since O<sub>3</sub> is removed from the sample stream, this SO<sub>2</sub> sonde avoids the compounded uncertainties of the dual-sonde method. Field deployments of the SO<sub>2</sub> sonde include sampling of volcanic emissions from Kīlauea on the big island of Hawai'i, US, and Turrialba volcano in Costa Rica and the emissions from petroleum extraction and processing at the Athabasca oil sands in Canada. Results from these field tests, covering a wide range of SO<sub>2</sub> concentrations from both natural and anthropogenic emission sources, are described below. The SO<sub>2</sub> sonde has been used for tethered and free-release balloons but can also be adapted for UAV platforms.

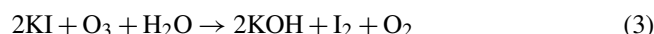
## 2 Instrumentation

### 2.1 Ozonesondes

The standard and modified ECC En-Sci ozonesondes were used for the O<sub>3</sub> and SO<sub>2</sub> sonde measurements in this study. The basic functioning of the ECC ozonesonde is described in Komhyr (1969) and Morris et al. (2010). The ECC sensor is composed of platinum cathode and anode electrodes, each in its own cell, immersed in a diluted and saturated solution of potassium iodide (KI), respectively. The cells are connected by an ion bridge allowing for the transfer of electrical charges while maintaining the separation of the solutions (Eqs. 1 and 2). When the cells are charged with the solution, a transient potential difference is generated that is dissipated through the redistribution of charge across the ion bridge. The following equilibria are established from these reactions:



Sampled air is pumped into the cathode cell, and the presence of O<sub>3</sub> initiates a reaction (Eq. 3) that causes an imbalance in favor of [I<sub>2</sub>] in the cathode solution.

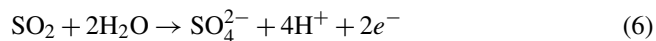


To rebalance the electrochemical potential of the cell, the iodine and iodide redox reactions in Eqs. (4) and (5) result in a flow of electrons from the anode to the cathode via the ion

bridge. This cell current, measured by an external ammeter, is proportional to the O<sub>3</sub> concentration.



When SO<sub>2</sub> is present in the sample air, an additional reaction (Eq. 6) occurs in the cathode cell of the ECC, supplying the two electrons needed to rebalance the cathode cell after the O<sub>3</sub> reaction (Eq. 3) (Komhyr, 1969; Morris et al., 2010).



Thus, each SO<sub>2</sub> molecule in the sampled air has the effect of canceling the measurement of one O<sub>3</sub> molecule. In effect, the standard ECC ozonesonde reports [O<sub>3</sub>] – [SO<sub>2</sub>] for its measurement. In most places and at most times, [SO<sub>2</sub>] ≪ [O<sub>3</sub>], so there is not a significant impact on the O<sub>3</sub> measurements, but in places downwind of SO<sub>2</sub> sources (e.g., coal-burning power plants or volcanoes), the O<sub>3</sub> measurement will be negatively impacted.

## 2.2 Instrumentation

Several SO<sub>2</sub> and O<sub>3</sub> instruments were used for validation of the SO<sub>2</sub> sonde during laboratory and field testing. A calibration system was used to produce controlled concentrations of SO<sub>2</sub> and O<sub>3</sub>. The calibration system relied on the operation of flow controllers or restrictors, an SO<sub>2</sub> ultra-high-purity (UHP) gas cylinder (4.87 ppm; Scott-Marrin, Inc., Riverside, CA) and/or a UV photometric O<sub>3</sub> calibrator (49C PS; Thermo Fisher Scientific, Franklin, MA), and zero air to produce desired pre-set concentrations of SO<sub>2</sub> and/or O<sub>3</sub>. The zero-air setup used for the field and laboratory testing was achieved using a dry zero-air UHP gas cylinder or else generated by scrubbing ambient air through activated charcoal and Purafil SP (Purafil, Inc., Doraville, GA) canisters. The Thermo 43i-TL SO<sub>2</sub> analyzer (LLOD: 60–90 pptv at 5 min averaging) and the 49i O<sub>3</sub> analyzer (LLOD: 1.5 ppbv at 5 min averaging) were also used during laboratory testing, while a Thermo 43c-TL SO<sub>2</sub> analyzer was used during field testing in Hawai'i. These instruments were set to report 10 s average measurements.

## 3 Single-sonde SO<sub>2</sub> system and laboratory testing

### 3.1 SO<sub>2</sub> sonde system description

The single-sonde SO<sub>2</sub> system included three major modifications to the En-Sci ECC ozonesonde: (1) the application of a positively biased current to the cathode cell, (2) the addition of an O<sub>3</sub> removal filter, and (3) a sample dryer (Fig. S1). The first version of the SO<sub>2</sub> system (SO<sub>2</sub> sonde v1.0) included the first two modifications: the bias current and an O<sub>3</sub> removal filter. The bias current sets the upper limit of detection (ULOD) for the SO<sub>2</sub> sonde and is set prior to measurement. The O<sub>3</sub> removal filter is placed in line with the inlet,

allowing O<sub>3</sub>-free air to be sampled in the SO<sub>2</sub> sonde. In the ECC, O<sub>3</sub> produces a positive response signal while SO<sub>2</sub> produces a negative signal when sufficient O<sub>3</sub> is present (i.e., positive signal). With these two modifications, SO<sub>2</sub> can be measured directly as the reduction of the cell current from the pre-set biased current (Flynn and Morris, 2021). Unlike the dual-sonde system, this approach allows for direct SO<sub>2</sub> measurements rather than an inference by subtraction of signals from two separate instruments. A sample dryer was added to the SO<sub>2</sub> sonde in the second version (v1.1) to combat humidity issues discovered after initial field tests. The addition of the dryer corrected the highly varying instrument sensitivity observed in the field. All components of the SO<sub>2</sub> sonde fit within a standard ozonesonde foam box (approximately 8 in. × 8 in. × 10 in.) except for the inlet filter. The free-release balloon payload's total mass is approximately 1 kg. The patent publication and Fig. S1 provide a detailed description and schematic of the SO<sub>2</sub> sonde (Flynn and Morris, 2021).

### 3.2 Testing of the bias current

The bias current is supplied by inserting into the cathode cell an additional platinum electrode powered by a 9 V battery (Fig. S1) (Flynn and Morris, 2021). To maintain consistent power, the circuit uses a 5 V regulator. Varying the resistance allows for a range of bias currents to be introduced. The current version of the SO<sub>2</sub> sonde uses a fixed resistor which requires a priori knowledge of the desired SO<sub>2</sub> concentration range. The desired resistor is installed in series with the battery and the electrode. An earlier laboratory test compared the SO<sub>2</sub> sonde measurements (initially configured without an O<sub>3</sub> removal filter) to those made by a 43i-TL SO<sub>2</sub> analyzer (Fig. 1, Table 1). O<sub>3</sub> and SO<sub>2</sub> gases were introduced using the laboratory calibration setup and a manifold to allow the sonde and the Thermo trace gas instruments to sample the same air. Results in Fig. 1 show 60 s averaged data. The test included (A) input of O<sub>3</sub> without an added bias current; (B) the same input of O<sub>3</sub> with the addition of a bias current (equivalent to approximately 90 ppbv of O<sub>3</sub>); and the addition of SO<sub>2</sub> to the O<sub>3</sub> with the enhanced bias signal where the SO<sub>2</sub> concentration was either (C) smaller or (D and E) larger than the O<sub>3</sub> concentration. During (A), measurements made by O<sub>3</sub> and SO<sub>2</sub> sondes compare well to measurements made by the Thermo instruments (Fig. 1, Table 1). The test included (E) the response of the SO<sub>2</sub> sonde to a reduction of the O<sub>3</sub> concentration, resulting in an equivalent decrease in signal, followed by (G–I) a reduction in the SO<sub>2</sub> concentration, resulting in an equivalent increase in signal. At (F), the SO<sub>2</sub> concentration exceeded the bias current (90 ppbv), producing a signal equivalent to  $2.9 \pm 0.1$  ppbv. The sonde successfully measured SO<sub>2</sub> both with and without O<sub>3</sub> with approximately 97 % efficiency.

Examination of the SO<sub>2</sub> sonde data showed that noise was proportional to the measured signal, with 1-σ noise at ap-

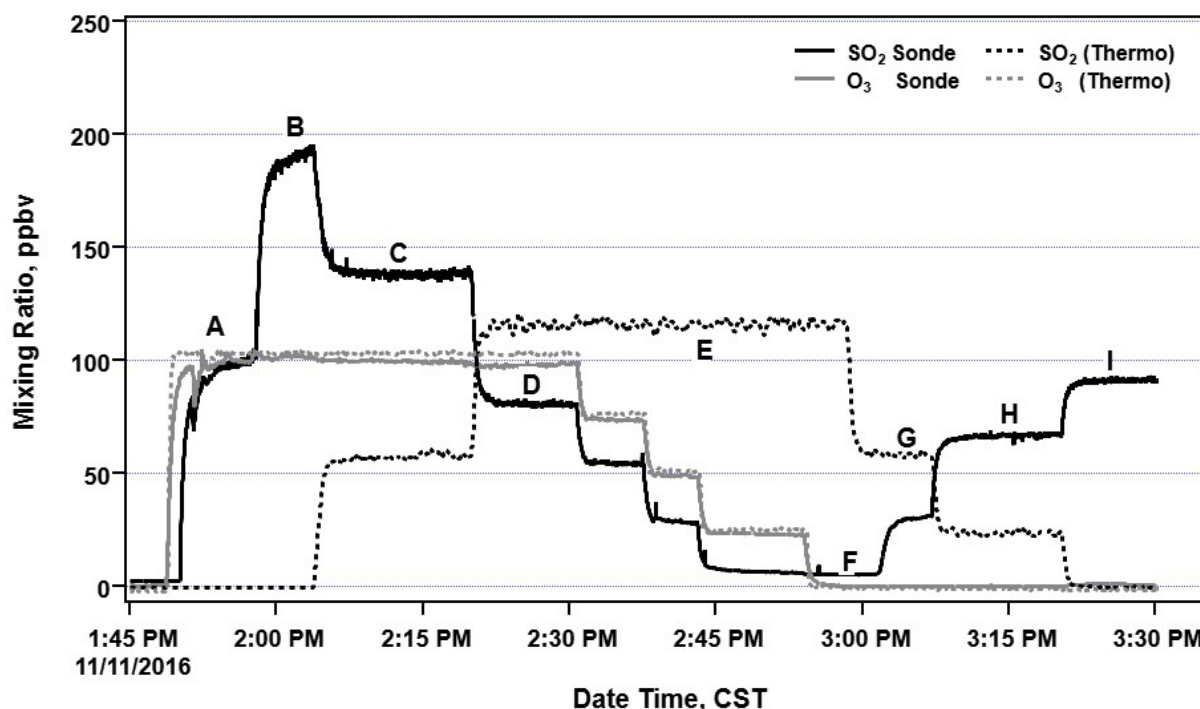


**Figure 1.** Test of the SO<sub>2</sub> sonde v1.0 (without an O<sub>3</sub> removal filter) with an applied bias current responding to O<sub>3</sub> and SO<sub>2</sub>. See the text for further details.

**Table 1.** Averaged O<sub>3</sub> and SO<sub>2</sub> concentration measured by the SO<sub>2</sub> sonde version 1.0 and Thermo instruments during different stages of testing indicated in Fig. 1.

|   | O <sub>3</sub> thermo (ppbv) | O <sub>3</sub> sonde (ppbv) | SO <sub>2</sub> thermo (ppbv) | SO <sub>2</sub> sonde (ppbv) |
|---|------------------------------|-----------------------------|-------------------------------|------------------------------|
| A | 105 ± 0.4                    | 100 ± 1.3                   | 0.0 ± 0.06                    | 96 ± 1.3                     |
| B | 105 ± 0.5                    | 101 ± 0.4                   | 0.0 ± 0.06                    | 188 ± 2.3                    |
| C | 103 ± 0.4                    | 99 ± 0.4                    | 57 ± 0.37                     | 135 ± 1.0                    |
| D | 105 ± 0.5                    | 97 ± 0.6                    | 116 ± 1.9                     | 78 ± 1.0                     |
| E | –                            | –                           | –                             | –                            |
| F | 1.3 ± 0.5                    | −0.13 ± 0.08                | 116 ± 1.4                     | 2.9 ± 0.1                    |
| G | 1.1 ± 0.4                    | −0.51 ± 0.11                | 58 ± 0.7                      | 29 ± 0.5                     |
| H | 0.61 ± 0.39                  | 0.15 ± 0.03                 | 24 ± 0.8                      | 64 ± 0.6                     |
| I | 0.31 ± 0.31                  | 0.64 ± 0.27                 | 0.25 ± 0.22                   | 89 ± 0.6                     |

proximately 0.2 %–0.3 % of the measured signal. Because increases in the SO<sub>2</sub> concentrations result in decreases in the signal (i.e., lower cell currents), the magnitude of the applied bias current determines the saturation point (i.e., ULOD) of the SO<sub>2</sub> sonde; saturation occurs when the measured cell current drops to zero. Applying a higher bias current increases the ULOD but also increases noise and the LLOD. The reported LLODs of bias currents are calculated as  $3\sigma$  relative to the baseline signal when sampling zero air. During laboratory testing, the LLOD ( $3\sigma$ ) was calculated for a range of applied bias currents (0.25 to 10.0  $\mu$ A). The LLOD for the varying bias current of 0.25 to 10.0  $\mu$ A ranged from approximately

0.002 to 0.084  $\mu$ A, respectively. Results of calculated LLOD of a 0.25  $\mu$ A bias current at varying replicated altitudes are included in Table S1 in the Supplement. At the surface, the LLOD of 20 s averaged measurements is 0.17 ppbv. The final version of the SO<sub>2</sub> sonde (v1.1) requires the bias current to be selected prior to measurement. If the bias current is set too low, a measurement of larger-than-expected SO<sub>2</sub> concentrations can saturate the sensor while a bias current that is set too high will have higher LLOD due to the increase in noise. The applied magnitude of the bias current can be best determined based on known SO<sub>2</sub> sources including volcanic emissions and urban and/or industrial emissions.

### 3.3 Testing of O<sub>3</sub> removal filter

Since the ECC responds to both O<sub>3</sub> and SO<sub>2</sub>, an O<sub>3</sub> removal filter was developed to remove interference from O<sub>3</sub> in the sample. This proprietary O<sub>3</sub> removal filter is placed upstream of the sonde inlet (Flynn and Morris, 2021). During laboratory testing, the O<sub>3</sub> removal filter was exposed to a continual concentration of  $487 \pm 3$  ppbv of O<sub>3</sub> and a varying concentration of SO<sub>2</sub> ranging from 0 to  $111 \pm 1$  ppbv (Fig. 2). The O<sub>3</sub> was effectively and consistently removed from the sampled air by the O<sub>3</sub> removal filter as SO<sub>2</sub> was diluted. The testing included measurements with (gray background) and without (white background) the O<sub>3</sub> removal filter. The SO<sub>2</sub> and O<sub>3</sub> concentrations measured by the Thermo 43i–TL and 49i instruments, respectively, and changes in SO<sub>2</sub> dilution levels are also indicated in Fig. 2. The O<sub>3</sub> removal filter de-

stroyed the O<sub>3</sub> at all SO<sub>2</sub> dilution levels to below the detection limit of the O<sub>3</sub> instrument. By comparing the Thermo 43i-TL SO<sub>2</sub> analyzer measurements with and without the O<sub>3</sub> removal filter, SO<sub>2</sub> passed through the filter with 88 % efficiency (Fig. 3a). The transmission efficiency was calculated by taking the ratio of SO<sub>2</sub> measured by the sonde to that measured by the analyzer. The SO<sub>2</sub> transmission efficiency increased to 97 % when testing the O<sub>3</sub> removal filter with the dry zero-air UHP gas cylinder (Fig. 3b) instead of the zero-air generator that processes ambient laboratory air (Fig. 3a). Additional testing of the O<sub>3</sub> removal filter demonstrated that the filter removed approximately 1 ppm of O<sub>3</sub> at sea level with > 99.9 % in O<sub>3</sub> removal efficiency, concentrations below the detection limit of the Thermo 49i O<sub>3</sub> monitor.

### 3.4 Sample dryer

The SO<sub>2</sub> sonde v1.0 had highly varying sensitivities during the initial field tests. The instrument sensitivity was determined by regression analysis of the sonde's cell current to the SO<sub>2</sub> concentration measured by an SO<sub>2</sub> analyzer. The variability in the sensitivities was hypothesized to be due to differing levels of humidity during each SO<sub>2</sub> sonde launch. SO<sub>2</sub> is soluble in water and through multiphase reactions can be oxidized to sulfuric acid in the atmosphere in the presence of water vapor (e.g., precipitation, clouds, fog) (Carmichael and Peters, 1979; Zhang et al., 2013; Terraglio and Manganelli, 1967). Factors including liquid water content, aerosol composition, aerosol loading, and pH of the water are important in determining the adsorption and oxidation rates of SO<sub>2</sub> (Liu et al., 2021). When air with elevated humidity is flowing through a filter, SO<sub>2</sub> gas is likely adsorbing on the filter, causing lower SO<sub>2</sub> transmission efficiency due to the potential uptake of SO<sub>2</sub> in water on the filter. Several laboratory tests confirmed the need to remove water from the sample upstream of the O<sub>3</sub> removal filter to improve the measurement of SO<sub>2</sub>. A desiccant membrane dryer (Perma Pure LLC, Lakewood, NJ) composed of a Nafion™ tube in silica gel desiccant was placed in-line upstream of the O<sub>3</sub> removal filter. This sample dryer is lightweight, relatively inexpensive, and does not require power.

Laboratory tests included exposing the SO<sub>2</sub> sonde, with and without a sample dryer, to controlled levels of humidity and SO<sub>2</sub>. Without removing water vapor, the SO<sub>2</sub> transmission efficiency decreases as humidity increases, particularly above 50 % RH (Fig. 6). As the O<sub>3</sub> removal filter is humidified, the SO<sub>2</sub> transmission efficiency decreases. With the sample dryer in place, each of the laboratory SO<sub>2</sub> transmission efficiency (17–18 and 21 May 2018) tests varied by an average of < 1 % across a range of 0 %–85 % RH (Fig. 6).

The dryer's useful lifetime was determined by continuously exposing it to high-humidity (> 95 % RH at approximately 23 °C) sample stream. The downstream RH climbed from 5 % to 16 % after 2.3 h and to 25 % after 6.3 h. At these downstream RH levels, the SO<sub>2</sub> transmission efficiency re-

mained above 95 %. A typical SO<sub>2</sub> sonde's measurement time per flight, including pre-flight calibration, is approximately 3 h. The dryer's useful lifetime is likely much longer than required for a balloon flight since exposure to 95 % RH conditions for several hours is highly unusual outside of hurricanes and tropical systems. SO<sub>2</sub> sonde and Thermo 43c-TL measurements were strongly correlated ( $r^2 = 0.99$ ) during a multipoint calibration conducted using the O<sub>3</sub> removal filter and the dryer under relatively high humidity levels. During that calibration, the SO<sub>2</sub> sonde's sensitivity was  $45.43 \pm 0.17$  ppbv  $\mu\text{A}^{-1}$ . By comparison, the average sensitivity during the initial Hawaii deployment was  $84.6 \pm 31.7$  ppbv  $\mu\text{A}^{-1}$  across 10 sondes. The sample dryer, therefore, improved both the sensitivity and stability of the measurements observed. The addition of the sample dryer is necessary for providing accurate ambient SO<sub>2</sub> measurements.

## 4 Field deployments with SO<sub>2</sub> sonde v1.0

The SO<sub>2</sub> sonde v1.0, single-SO<sub>2</sub> sonde without the sample dryer, was deployed and tested in Hawai'i and Costa Rica (Fig. S2). The field sites were close to active volcanoes, which are significant sources of natural SO<sub>2</sub> (Tang et al., 2020; Carn et al., 2017). In Hawai'i, field measurements were made near Kīlauea volcano on the southeastern shore of the island of Hawai'i, the largest of Hawai'i's islands. Kīlauea is the youngest volcano on the island and one of Earth's most active volcanoes (Kern et al., 2015; Nadeau et al., 2015). Kīlauea had been in a state of eruption since 1983 (Patrick et al., 2019), with an average SO<sub>2</sub> release rate of approximately  $5500 \text{ T d}^{-1}$  measured during 2014–2017 (Elias et al., 2018). In Costa Rica, field measurements were made near Turrialba volcano, one of the most active volcanoes in the Central American Volcanic Arc. Studies of emissions from Turrialba prior to 2013 reported SO<sub>2</sub> release rates of up to  $4000 \text{ T d}^{-1}$  (de Moor et al., 2016; Xi et al., 2016). The activity of Turrialba increased after 2014, raising concerns for air quality and environmental health (de Moor et al., 2016; Tortini et al., 2017).

### 4.1 Kīlauea, Hawai'i – February 2018

The first deployment of the SO<sub>2</sub> sonde v1.0 was during NASA's HypIRI HyTES Hawaii Campaign (H3C) from 3–10 February 2018, near Kīlauea volcano. The instrument was tested in flights on free-release balloons and a tethered balloon system (TBS) and at ground level with measurements in Hawai'i Volcanoes National Park (HVNP) downwind of Kīlauea's summit crater, Halema'uma'u. During the ground-level testing, an SO<sub>2</sub> sonde and a Thermo 43c-TL SO<sub>2</sub> analyzer's sample inlet were mounted on the top of a van for co-located sampling.

Figure 4a depicts the measurements taken during the first encounter with an SO<sub>2</sub> plume while driving through

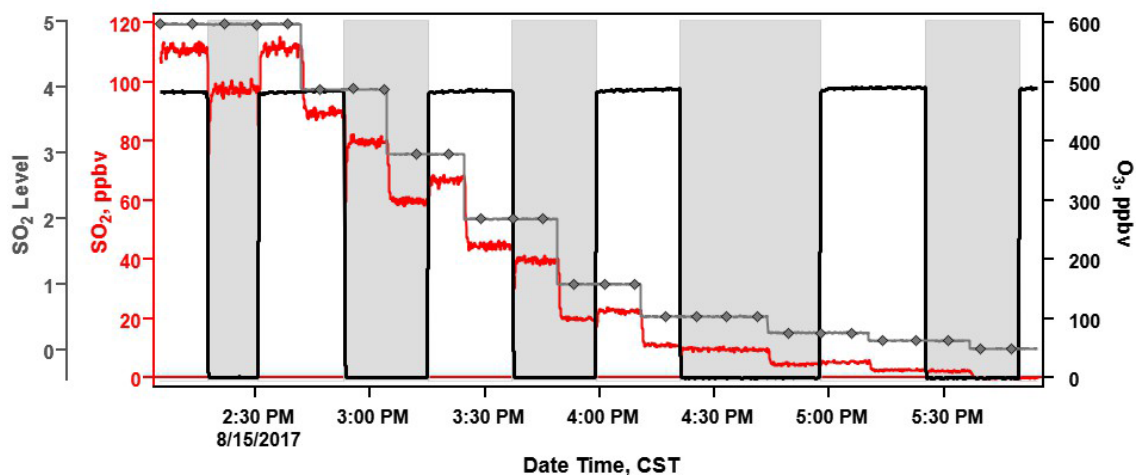


**Figure 2.** Time of series of a multipoint test of the O<sub>3</sub> filter removal efficiency and impact on SO<sub>2</sub> measurements taken by a Thermo 43i-TL SO<sub>2</sub> analyzer. Changes in SO<sub>2</sub> dilution levels are indicated by the pink lines (diamond markers).

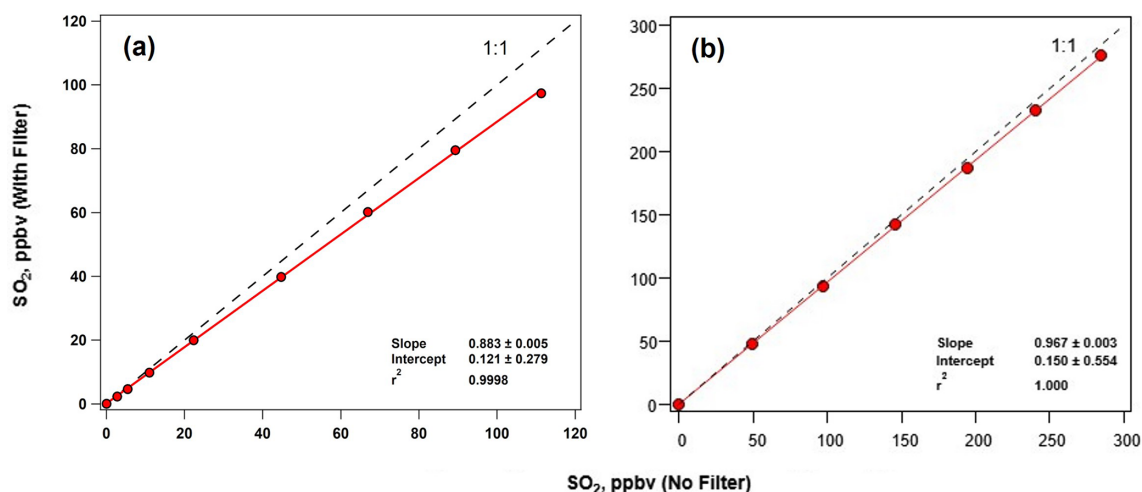


**Figure 3.** Response of Thermo 43i-TL SO<sub>2</sub> analyzer with (y axis) and without (x axis) an O<sub>3</sub> removal filter using a calibration system with (a) a processed zero-air system and (b) a dry zero-air gas cylinder.

the HVNP on 3 February 2018. The strongly correlated SO<sub>2</sub> sonde and Thermo 43c-TL measurements ( $r^2 = 0.99$ ) reached upward of  $\sim 940$  ppbv. The SO<sub>2</sub> sonde had a sensitivity of  $118.4 \pm 0.4$  ppbv  $\mu\text{A}^{-1}$ , determined by regression analysis of the sonde's cell current with the Thermo 43c-TL concentrations (Fig. 4a). The SO<sub>2</sub> sonde sensitivity varied significantly during the field deployment. During surface measurements on 10 February 2018, earlier zero-air calibrations measured a sensitivity of  $86.5 \pm 1.5$  ppbv  $\mu\text{A}^{-1}$ , while measurements during an SO<sub>2</sub> plume event, with peak concentrations of up to 400 ppbv, found the SO<sub>2</sub> sonde's sensitivity was  $73.9 \pm 0.6$  ppbv  $\mu\text{A}^{-1}$  (Fig. 4b). Although the SO<sub>2</sub> sonde sensitivity varied significantly in 10 subsequent calibrations ( $84.6 \pm 31.7$  ppbv  $\mu\text{A}^{-1}$ ), the measurements remained strongly correlated (range:  $r^2 = 0.94$ – $0.99$ ). The variability in the sensitivity in the field was due to

changes in the ambient RH impacting the SO<sub>2</sub> transmission efficiency of the O<sub>3</sub> removal filter. This hypothesis was confirmed by laboratory RH testing and discussed in Sect. 3.3 and 3.4.

#### 4.2 Turrialba, Costa Rica (dual-sonde versus SO<sub>2</sub> sonde comparison)

On 23 March 2018, a traditional SO<sub>2</sub> dual-sonde payload (Morris et al., 2010) and the SO<sub>2</sub> sonde v1.0 were launched using a free-release balloon flight from the Universidad de Costa Rica's campus in San Jose (approximately 31 km downwind of Turrialba volcano). This flight provided the first direct in situ comparison of the two SO<sub>2</sub> sonde methods. Figure 5 shows the response of the SO<sub>2</sub> sonde v1.0 and the calculated SO<sub>2</sub> dual-sonde profile. The dual-sonde SO<sub>2</sub>



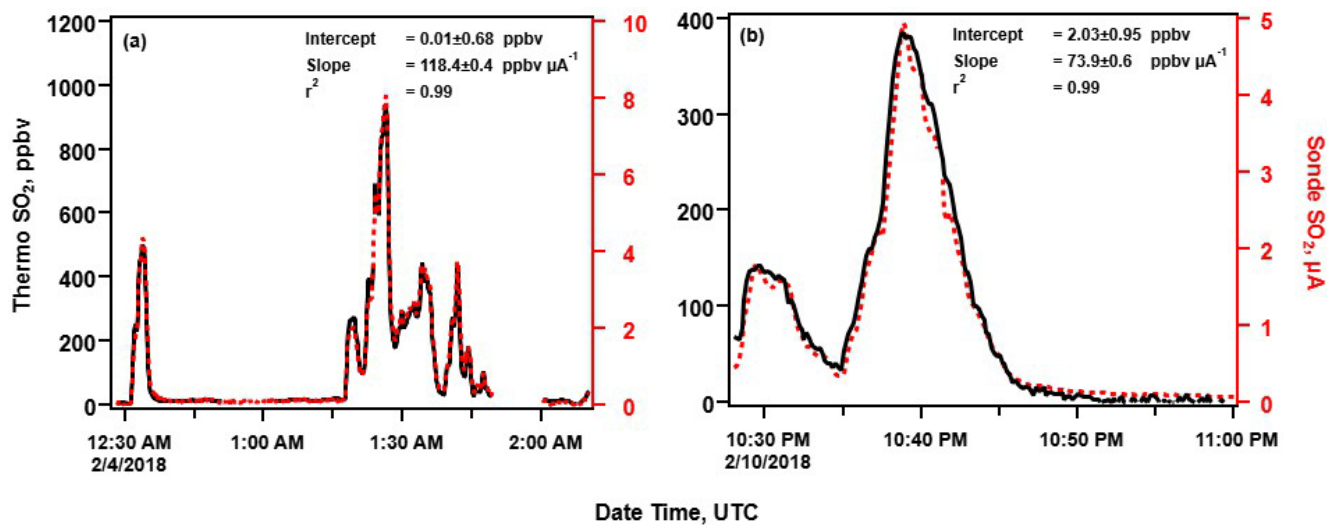


**Figure 4.** SO<sub>2</sub> sonde v1.0 and Thermo Environmental SO<sub>2</sub> analyzer measurements at Kīlauea, Hawai‘i, during H3C for (a) initial SO<sub>2</sub> plume encounter on 3 February 2018 and (b) a pre-flight measurement on 10 February 2018, approximately 6 km downwind of Kīlauea’s summit crater.

method can only report concentrations of SO<sub>2</sub> up to a maximum of the concentration of O<sub>3</sub> present. Furthermore, because the SO<sub>2</sub> concentration is determined by subtracting the signals from two instruments, its uncertainty is higher than the uncertainty of a measurement from a single instrument. When [SO<sub>2</sub>] > [O<sub>3</sub>], the dual sonde’s unfiltered ozonesonde signal goes to zero, as happened for the Turrialba sonde launch between 3 and 5 km (Fig. 5). The SO<sub>2</sub> saturates the cathode solution in the unfiltered sonde, not recovering until enough ambient O<sub>3</sub> has been processed to rebalance the cell, resulting in a distorted profile (Fig. 5). For this flight, the SO<sub>2</sub> sonde was configured to its maximum range (ULOD of approximately 450 ppbv at standard pressure) and was able to capture both the small plume below 2 km above mean sea level (a.m.s.l.) (approximately 18 ppbv) and the primary plume between 3 and 4 km a.m.s.l. (approximately 230 ppbv). The SO<sub>2</sub> sonde v1.0 was able to capture the full shape of the profile, including the peak values and structure of the plume. The SO<sub>2</sub> sonde v1.0 reports the top of the plume around 4 km a.m.s.l., whereas the dual sonde remains saturated until closer to 5 km a.m.s.l. Thus, the dual-sonde SO<sub>2</sub> profiles, when saturated by high concentrations of SO<sub>2</sub>, erroneously appear to have a greater vertical extent. Further, the SO<sub>2</sub> sonde v1.0 showed no interference from O<sub>3</sub> at altitudes from the surface to 24.4 km a.m.s.l., with O<sub>3</sub> concentrations in the stratospheric O<sub>3</sub> layer reaching > 4 ppmv (not shown), demonstrating the effectiveness of the O<sub>3</sub> filter. The SO<sub>2</sub> VCD was 8.3 DU (Dobson units, 1 DU = 2.69 × 10<sup>16</sup> molec. cm<sup>-2</sup>) for the SO<sub>2</sub> sonde but was only 3.4 DU for the dual-sonde measurement. Thus, once saturated, the dual-sonde method is likely to underestimate the SO<sub>2</sub> VCD.

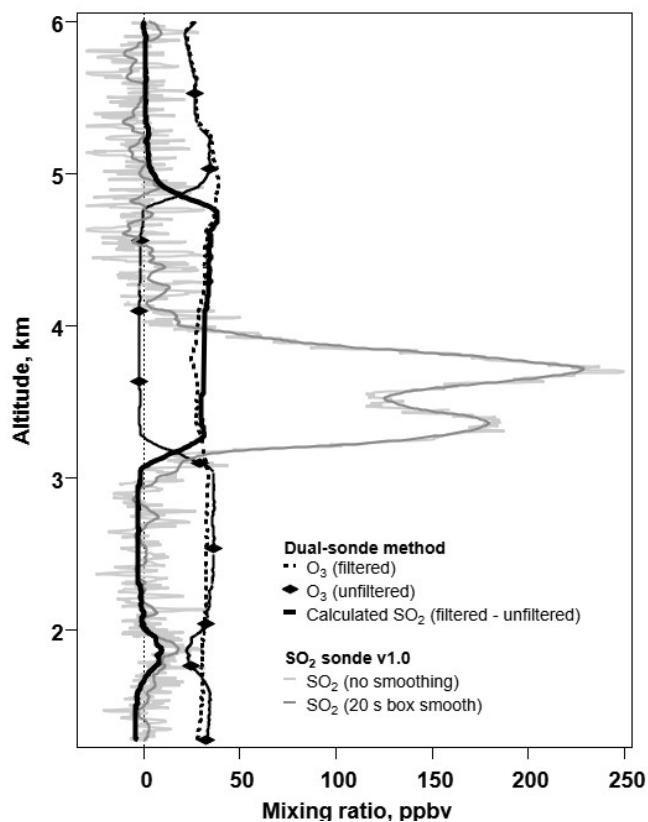


**Figure 5.** The profiles of a triple-sonde payload, which consisted of a dual sonde in tandem with an SO<sub>2</sub> sonde v1.0, launched from the Universidad de Costa Rica’s campus in San Jose (approximately 31 km downwind of the volcano Turrialba) on 23 March 2018.

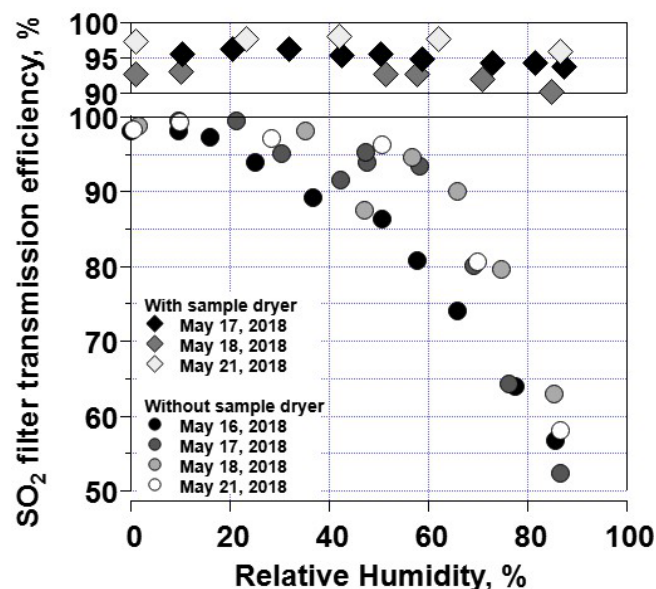


**Figure 6.** Tests of SO<sub>2</sub> transmission efficiency as a function of relative humidity without (circles) and with (diamonds) an upstream sample dryer.

## 5 Field deployments with SO<sub>2</sub> sonde v1.1

The updated SO<sub>2</sub> sonde (SO<sub>2</sub> sonde v1.1) with the dryer filter was deployed and tested near Ft. Mackay, Canada, and again in Hawai'i in June 2018. Ft. Mackay is in the Alberta province of Canada and is home to the Athabasca oil sands, a large area of bitumen and heavy crude oil surface deposits high in sulfur content. Local processing of these products (e.g., surface mining) and resulting byproducts (e.g., tailing ponds) can release significant amounts of SO<sub>2</sub> into the atmosphere (Bari et al., 2020; McLinden et al., 2016; Simpson et al., 2010). A second field deployment to Hawai'i followed immediately after the deployment to Canada. On 3 May 2018, Kīlauea volcano on Hawai'i entered a new eruptive phase with an outbreak of a series of fissures in the lower Puna area (Liu et al., 2021; Anderson et al., 2019; Gansecki et al., 2019; Patrick et al., 2020). The active phase volcanic gas emissions resulted in localized evacuations in the Lower East Rift Zone (LERZ), destroying more than 700 homes and displacing thousands of residents, and resulting in poor air quality for much of the southern and western portions of the island (Tang et al., 2020). The eruption event entered a paused phase in early August and was declared over on 5 December 2018 (Kern et al., 2020).

### 5.1 Athabasca oil sands, Canada

The SO<sub>2</sub> sonde v1.1 was tested in Ft. Mackay (57.1206° N, 111.4241° W), Alberta, in the Athabasca oil sands from 10–16 June 2018 (Fig. S2c). This field project, conducted in conjunction with Environment Canada and York University,

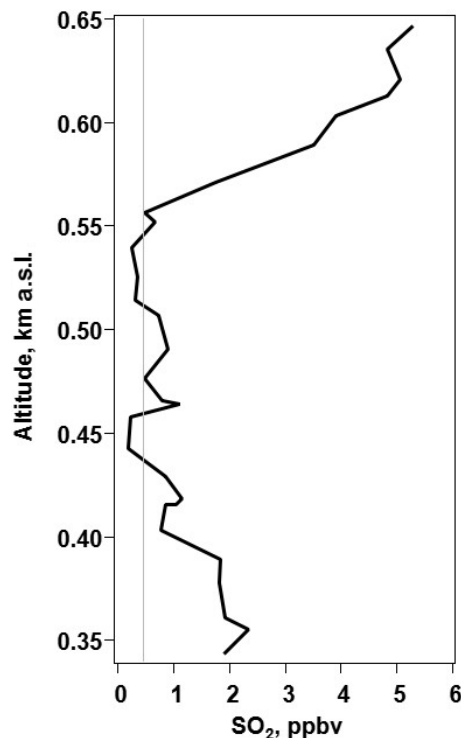


**Figure 7.** The profile, constructed using 20 s average changes in altitude (ranging from 1 to 15 km), is for a tethered SO<sub>2</sub> sonde v1.1 in the Athabasca oil sands region of Alberta, Canada. The SO<sub>2</sub> sonde bias current was 0.5  $\mu$ A, and the LLOD was 0.47 ppbv.

evaluated SO<sub>2</sub> emissions from industrial activities in and near the oil sands region using a combination of TBS and ground-based measurements. The SO<sub>2</sub> sonde v1.1 was flown on the York TBS payload, recording measurements from the ground to 300 m above ground level (a.g.l.; 650 m a.m.s.l.). This deployment provided a dilute anthropogenic plume to test the SO<sub>2</sub> sonde in a high-sensitivity, low-range configuration. The average sensitivity of the SO<sub>2</sub> sonde v1.1 during the project was  $51 \pm 1.2$  ppbv  $\mu$ A<sup>-1</sup>. The SO<sub>2</sub> sonde was configured to sample in a range from  $\sim 0.5$ –25 ppbv of SO<sub>2</sub>. The TBS SO<sub>2</sub> sonde's vertical profiles were averaged into 10 m altitude bins that measured SO<sub>2</sub> concentration ranges that are more representative of anthropogenically impacted SO<sub>2</sub> rather than large volcanic plumes (Fig. 7). This field deployment also demonstrated the performance of the sonde at sub-ppbv levels of ambient SO<sub>2</sub>.

### 5.2 Kīlauea, Hawai'i – June 2018

In response to the larger eruption that started in May 2018, the SO<sub>2</sub> sonde v1.1 was deployed to Hawai'i for the NASA-funded Big Island SO<sub>2</sub> Survey (BISOS). The SO<sub>2</sub> sonde launches occurred from Kahuku Ranch (19.0549° N, 155.6934° W) and Na'alehu Elementary School (19.0610° N, 155.5788° W) approximately 90 km



**Table 2.** The SO<sub>2</sub> vertical column density (VCD) for profiles shown in Fig. 8 from BISOS in June 2018. For profile c, the descent profile VCD is reported for the flight without extrapolation (shown without parentheses) and using linear extrapolation assuming the SO<sub>2</sub> concentration to be 0 ppbv at sea level (shown in parentheses).

| Profile     | Launch time (UTC)  | SO <sub>2</sub> VCD        |
|-------------|--------------------|----------------------------|
| a (ascent)  | 22 June 2018 00:32 | 8.6 DU                     |
| b (ascent)  | 28 June 2018 20:45 | 12.5 DU                    |
| c (descent) | 29 June 2018 21:36 | 6.2 (9.8 <sup>a</sup> ) DU |
| d (ascent)  | 30 June 2018 20:48 | 79.1 DU <sup>b</sup>       |

<sup>a</sup> VCD from extrapolated data. <sup>b</sup> Saturation of SO<sub>2</sub> at altitudes of 1 to 3 km a.m.s.l.

downwind of Kīlauea's LERZ (Fig. S2d). The site's distance from the source allowed the plume to disperse and dilute compared with measurements at the vent. An SO<sub>2</sub> plume was detected during seven of the nine free-release balloon launches during the June 2018 BISOS campaign. The 10 SO<sub>2</sub> sonde v1.1 calibrations performed during BISOS had an SO<sub>2</sub> sensitivity of  $47.0 \pm 5.8$  ppbv  $\mu\text{A}^{-1}$  and were similar to the laboratory results ( $45.43 \pm 0.17$  ppbv  $\mu\text{A}^{-1}$ ).

With the anticipated levels of SO<sub>2</sub>, the sondes were configured to sample in the range of 10–450 ppbv of SO<sub>2</sub>. Figure 8 shows four distinctive SO<sub>2</sub> profiles, and Table 2 includes the VCDs for each flight. No plumes above 5 km a.m.s.l. were detected. All but one of the observed SO<sub>2</sub> plumes were below the capping inversion of the planetary boundary layer (PBL). On 22 June (Fig. 8a), the ascent profile shows SO<sub>2</sub> below 3 km a.m.s.l. peaking at nearly 100 ppbv and additional features between 3 and 4 km a.m.s.l. peaking at 20–35 ppbv (Tang et al., 2020). The latter peaks were correlated with higher RH, perhaps the result of steam from a vent or the ocean entry points having broken through the inversion. The early afternoon 28 June profile (Fig. 8b) shows the highest concentration (325 ppbv) for a resolved SO<sub>2</sub> plume during the BISOS campaign. Typical for the trade winds, NOAA HYSPLIT trajectories (Stein et al., 2015) showed the winds were out of the NE, consistent with the plume's transport from vents in the LERZ or the lava ocean entry points. Although the descent profile from a 29 June early afternoon launch lost the signal at 0.58 km a.m.s.l., Fig. 8c shows an SO<sub>2</sub> plume over the ocean with a peak concentration of 188 ppbv at 0.74 km a.m.s.l. HYSPLIT trajectories again showed the winds were out of the NE. Lastly, the SO<sub>2</sub> plume detected during the ascent of the 30 June launch (Fig. 8d) exceeded the ULOD between 1 and 3 km a.m.s.l. for the SO<sub>2</sub> sonde configuration used. The distorted SO<sub>2</sub> enhancement extending above the PBL as determined by the temperature inversion is most likely an artifact of the saturated sonde, similar to what was seen in the dual-sonde profile from Costa Rica (Fig. 5). As the RH remains low above the PBL, it is most likely that the SO<sub>2</sub> is contained entirely within the PBL.

## 6 Conclusion and future work

An innovative new method for measuring vertical profiles of SO<sub>2</sub> from TBS and free-release balloons was successfully tested and demonstrated in controlled laboratory experiments and during four different field deployments covering SO<sub>2</sub> concentrations ranging from 0.5–325 ppbv during flights and up to 940 ppbv during ground measurements. This new method requires three major modifications to the standard ECC ozonesonde: the addition of a positive bias current in the cathode cell, an O<sub>3</sub> removal filter, and a sample dryer. Relative to the previous dual-sonde method, the new method measures SO<sub>2</sub> using a single-sonde system (i.e., the SO<sub>2</sub> sonde). The SO<sub>2</sub> sonde and Thermo 43c-TL measurements were strongly correlated during laboratory ( $r^2 > 0.99$ ) and field-based ( $r^2 > 0.94$ ) comparisons. Initial field tests and subsequent laboratory testing of SO<sub>2</sub> sonde v1.0 highlighted the need to dry the sample upstream of the O<sub>3</sub> removal filter to achieve consistent results. Follow-up field measurements in the Athabasca oil sands and Hawai'i clearly demonstrated the improvement in the SO<sub>2</sub> sonde v1.1's sensitivity and consistency ( $51 \pm 1.2$  and  $47 \pm 5.8$  ppbv  $\mu\text{A}^{-1}$ , respectively) as a result of drying the sample.

The SO<sub>2</sub> sonde v1.1 offers several advantages over the dual-sonde method, including the ability to measure [SO<sub>2</sub>] independent of [O<sub>3</sub>], the capability of sub-ppbv detection limits, faster response and recuperation time when exposed to larger SO<sub>2</sub> plumes, and reduced uncertainty. The lighter weight of the payload requires a smaller balloon and less helium to lift, which may prove advantageous for deployment under some field conditions, particularly where helium supplies are limited. Its compactness and weight can also make it a candidate for UAV campaigns. Field deployments revealed specific issues and areas for improvement. The present design requires pre-setting the sonde's bias current prior to the launch. Thus, some a priori estimates of the plume are required to determine the appropriate bias current so that the instrument can measure the full range of SO<sub>2</sub> concentrations present. In the current SO<sub>2</sub> sonde v1.1, increasing the ULOD by applying a larger bias current also increases the LLOD. Further laboratory experiments are needed to identify the factors that cause the remaining observed variability in the SO<sub>2</sub> transmission efficiency in the latest instrument version that includes the sample dryer. Much of the testing and calibration completed to date assessed the complete SO<sub>2</sub> sonde system (i.e., sonde, filter, dryer). Building a database of the various individual factors, including pump speeds and filter transmission efficiency, will help us to better characterize the causes of sonde-to-sonde variability and allow future versions of the system to improve performance characteristics so that the system can be made available for operational use. Additionally, future paper topics include intercomparison studies of the SO<sub>2</sub> sonde's vertical profile measurements with other column measurements (i.e., Pandora) and satellite

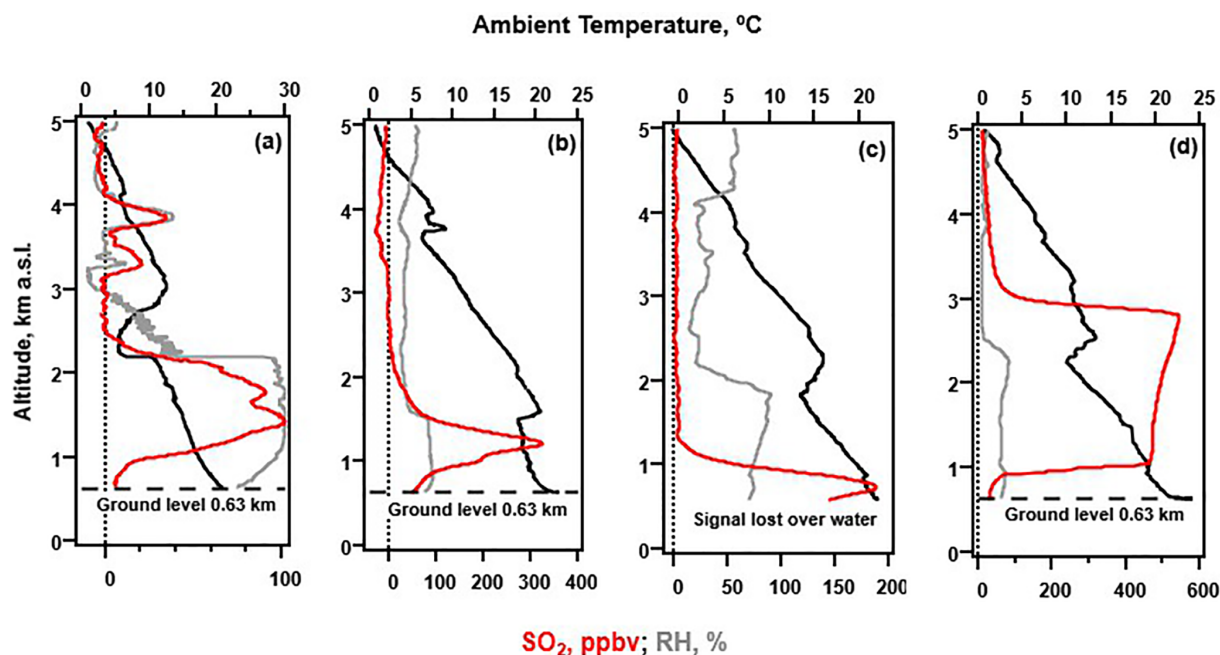


**Figure 8.** Vertical profiles of SO<sub>2</sub> (20 s box smoothing) from the SO<sub>2</sub> sonde v1.1 during BISOS in June 2018 with free-release balloon launches occurring at the Kahuku Ranch on the big island of Hawai'i. Profiles are from (a) 22 June 2018 00:32, (b) 28 June 2018 20:45, (c) 29 June 2018 21:36, and (d) 30 June 2018 20:48. All times are UTC.

measurements and more in-depth analysis of the SO<sub>2</sub> sonde measurements at the various field deployments.

*Data availability.* Data and code related to this article are available upon request to corresponding author.

*Supplement.* The supplement related to this article is available online at: <https://doi.org/10.5194/amt-15-4373-2022-supplement>.

*Author contributions.* JHF and GM conceptualized the study. JHF, AK, SLA, MGS, EK, PW, GM, EC, AA, and JAD curated the data. AK, SLA, SY, and PW performed the analysis. JHF acquired funding for the project. AK, SLA, MGS, and EK led the investigation of the study. JHF and GM designed the methodology. SY wrote and prepared the original draft of manuscript. PW, GM, JAD, and JHF reviewed and edited the manuscript. JHF supervised the project.

*Competing interests.* The contact author has declared that none of the authors has any competing interests.

*Disclaimer.* Publisher's note: Copernicus Publications remains neutral with regard to jurisdictional claims in published maps and institutional affiliations.

*Acknowledgements.* We especially appreciate our collaboration with En-Sci in advancing this work. We would also like to thank Mark Gordon of York University and David Tarasick of Environment Canada for their invitation and assistance with the deployment to Ft. Mackay and Henry Selkirk and Holger Vomel from the TicoSonde project for their support in the Turrialba volcano testing campaign. A special thanks to Principal Darlene Javar of Na'alehu Elementary School and its teachers, staff, and students for letting us install equipment on a roof and helping us with a launch. Also, we thank the two anonymous reviewers for helpful comments on the original draft of this paper.

*Financial support.* This research has been supported by the National Aeronautics and Space Administration (grant nos. NNG11HP16A and 80NSSC18K1061).

*Review statement.* This paper was edited by Hendrik Fuchs and reviewed by two anonymous referees.

## References

- Anderson, K. R., Johanson, I. A., Patrick, M. R., Gu, M., Segall, P., Poland, M. P., Montgomery-Brown, E. K., and Miklius, A.: Magma reservoir failure and the onset of caldera collapse at Kīlauea Volcano in 2018, *Science*, 366, eaaz1822, <https://doi.org/10.1126/science.aaz1822>, 2019.
- Bari, M. A., Kindzierski, W. B., and Roy, P.: Identification of ambient SO<sub>2</sub> sources in industrial areas in the lower Athabasca oil

- sands region of Alberta, Canada, *Atmos. Environ.*, 231, 117505, <https://doi.org/10.1016/j.atmosenv.2020.117505>, 2020.
- Bluth, G. J., Doiron, S. D., Schnetzler, C. C., Krueger, A. J., and Walter, L. S.: Global tracking of the SO<sub>2</sub> clouds from the June, 1991 Mount Pinatubo eruptions, *Geophys. Res. Lett.*, 19, 151–154, 1992.
- Carmichael, G. R. and Peters, L. K.: Some aspects of SO<sub>2</sub> absorption by water-generalized treatment, *Atmos. Environ.*, 13, 1505–1513, 1979.
- Carn, S., Fioletov, V., McLinden, C., Li, C., and Krotkov, N.: A decade of global volcanic SO<sub>2</sub> emissions measured from space, *Scientific Reports*, 7, 44095, <https://doi.org/10.1038/srep44095>, 2017.
- Chen, T.-M., Kuschner, W. G., Gokhale, J., and Shofer, S.: Outdoor air pollution: nitrogen dioxide, sulfur dioxide, and carbon monoxide health effects, *Am. J. Med. Sci.*, 333, 249–256, 2007.
- Delmelle, P., Stix, J., Baxter, P., Garcia-Alvarez, J., and Barquero, J.: Atmospheric dispersion, environmental effects and potential health hazard associated with the low-altitude gas plume of Masaya volcano, Nicaragua, *B. Volcanol.*, 64, 423–434, 2002.
- de Moor, J. M., Aiuppa, A., Avaró, G., Wehrmann, H., Dunbar, N., Müller, C., Tamburello, G., Giudice, G., Liuzzo, M., and Moretti, R.: Turmoil at Turrialba Volcano (Costa Rica): Degassing and eruptive processes inferred from high-frequency gas monitoring, *J. Geophys. Res.-Sol. Ea.*, 121, 5761–5775, 2016.
- Diaz, J. A., Pieri, D., Wright, K., Sorensen, P., Kline-Shoder, R., Arkin, C. R., Fladeland, M., Bland, G., Buongiorno, M. F., and Ramirez, C.: Unmanned aerial mass spectrometer systems for in-situ volcanic plume analysis, *J. Am. Soc. Mass Spectr.*, 26, 292–304, 2015.
- Elias, T., Kern, C., Horton, K. A., Sutton, A. J., and Garbeil, H.: Measuring SO<sub>2</sub> emission rates at Kīlauea Volcano, Hawaii, using an array of upward-looking UV spectrometers, 2014–2017, *Front. Earth Sci.*, 6, 214, <https://doi.org/10.3389/feart.2018.00214>, 2018.
- US EPA: National air quality and emissions trends, 1998, United States Environmental Protection Agency, EPA-454/R-00-003, 2000.
- Flynn, J. and Morris, G. A.: A method for directly measuring SO<sub>2</sub> and other trace gases by electrochemical cell (ECC) sonde, Patent, United States Patent 11,150,217, <https://patentimages.storage.googleapis.com/4e/b7/eb/6c08e69823abfa/US11150217.pdf> (last access: 28 February 2022), 2021.
- Galle, B., Johansson, M., Rivera, C., Zhang, Y., Kihlman, M., Kern, C., Lehmann, T., Platt, U., Arellano, S., and Hidalgo, S.: Network for Observation of Volcanic and Atmospheric Change (NOVAC)—A global network for volcanic gas monitoring: Network layout and instrument description, *J. Geophys. Res.*, 115, D05304, <https://doi.org/10.1029/2009JD011823>, 2010.
- Gansecki, C., Lee, R. L., Shea, T., Lundblad, S. P., Hon, K., and Parcheta, C.: The tangled tale of Kīlauea's 2018 eruption as told by geochemical monitoring, *Science*, 366, eaaz0147, <https://doi.org/10.1126/science.aaz0147>, 2019.
- Kern, C., Sutton, J., Elias, T., Lee, L., Kamibayashi, K., Antolik, L., and Werner, C.: An automated SO<sub>2</sub> camera system for continuous, real-time monitoring of gas emissions from Kīlauea Volcano's summit Overlook Crater, *J. Volcanol. Geoth. Res.*, 300, 81–94, 2015.
- Kern, C., Lerner, A. H., Elias, T., Nadeau, P. A., Holland, L., Kelly, P. J., Werner, C. A., Clor, L. E., and Cappos, M.: Quantifying gas emissions associated with the 2018 rift eruption of Kīlauea Volcano using ground-based DOAS measurements, *B. Volcanol.*, 82, 1–24, 2020.
- Kiehl, J. and Briegleb, B.: The relative roles of sulfate aerosols and greenhouse gases in climate forcing, *Science*, 260, 311–314, 1993.
- Komhyr, W.: Electrical concentration cells for gas analysis, *Ann. Geophys.*, 25, 203–210, 1969.
- Krug, E. C. and Frink, C. R.: Acid rain on acid soil: a new perspective, *Science*, 221, 520–525, 1983.
- Liu, T., Chan, A. W., and Abbatt, J. P.: Multiphase Oxidation of Sulfur Dioxide in Aerosol Particles: Implications for Sulfate Formation in Polluted Environments, *Environ. Sci. Technol.*, 55, 4227–4242, 2021.
- McLinden, C. A., Fioletov, V., Krotkov, N. A., Li, C., Boersma, K. F., and Adams, C.: A decade of change in NO<sub>2</sub> and SO<sub>2</sub> over the Canadian oil sands as seen from space, *Environ. Sci. Technol.*, 50, 331–337, 2016.
- Morris, G. A., Komhyr, W. D., Hirokawa, J., Flynn, J., Lefter, B., Krotkov, N., and Ngan, F.: A balloon sounding technique for measuring SO<sub>2</sub> plumes, *J. Atmos. Ocean. Tech.*, 27, 1318–1330, 2010.
- Nadeau, P. A., Werner, C. A., Waite, G. P., Carn, S. A., Brewer, I. D., Elias, T., Sutton, A. J., and Kern, C.: Using SO<sub>2</sub> camera imagery and seismicity to examine degassing and gas accumulation at Kīlauea Volcano, May 2010, *J. Volcanol. Geoth. Res.*, 300, 70–80, 2015.
- Parker, D. E., Wilson, H., Jones, P. D., Christy, J., and Folland, C. K.: The impact of Mount Pinatubo on world-wide temperatures, *Int. J. Climatol.*, 16, 487–497, 1996.
- Patrick, M., Orr, T., Anderson, K., and Swanson, D.: Eruptions in sync: Improved constraints on Kīlauea Volcano's hydraulic connection, *Earth Planet. Sc. Lett.*, 507, 50–61, 2019.
- Patrick, M., Johanson, I., Shea, T., and Waite, G.: The historic events at Kīlauea Volcano in 2018: summit collapse, rift zone eruption, and M<sub>w</sub> 6.9 earthquake: preface to the special issue, *B. Volcanol.*, 82, 46, <https://doi.org/10.1007/s00445-020-01377-5>, 2020.
- Pieri, D., Diaz, J. A., Bland, G., Fladeland, M., Madrigal, Y., Corrales, E., Alegria, O., Alan, A., Realmuto, V., and Miles, T.: In situ observations and sampling of volcanic emissions with NASA and UCR unmanned aircraft, including a case study at Turrialba Volcano, Costa Rica, Geological Society, London, Special Publications, 380, 321–352, 2013.
- Schmidt, A., Carslaw, K. S., Mann, G. W., Wilson, M., Breider, T. J., Pickering, S. J., and Thordarson, T.: The impact of the 1783–1784 AD Laki eruption on global aerosol formation processes and cloud condensation nuclei, *Atmos. Chem. Phys.*, 10, 6025–6041, <https://doi.org/10.5194/acp-10-6025-2010>, 2010.
- Shannon, J. D.: Regional trends in wet deposition of sulfate in the United States and SO<sub>2</sub> emissions from 1980 through 1995, *Atmos. Environ.*, 33, 807–816, 1999.
- Simpson, I. J., Blake, N. J., Barletta, B., Diskin, G. S., Fuelberg, H. E., Gorham, K., Huey, L. G., Meinardi, S., Rowland, F. S., Vay, S. A., Weinheimer, A. J., Yang, M., and Blake, D. R.: Characterization of trace gases measured over Alberta oil sands mining operations: 76 speciated C<sub>2</sub>–C<sub>10</sub> volatile organic compounds

- (VOCs), CO<sub>2</sub>, CH<sub>4</sub>, CO, NO, NO<sub>2</sub>, NO<sub>y</sub>, O<sub>3</sub> and SO<sub>2</sub>, *Atmos. Chem. Phys.*, 10, 11931–11954, <https://doi.org/10.5194/acp-10-11931-2010>, 2010.
- Stein, A. F., Draxler, R. R., Rolph, G. D., Stunder, B. J., Cohen, M. D., and Ngan, F.: NOAA's HYSPLIT atmospheric transport and dispersion modeling system, *B. Am. Meteorol. Soc.*, 96, 2059–2077, 2015.
- Sunyer, J., Atkinson, R., Ballester, F., Le Tertre, A., Ayres, J. G., Forastiere, F., Forsberg, B., Vonk, J., Bisanti, L., and Anderson, R.: Respiratory effects of sulphur dioxide: a hierarchical multi-city analysis in the APHEA 2 study, *Occup. Environ. Med.*, 60, e2, <https://doi.org/10.1136/oem.60.8.e2>, 2003.
- Tang, Y., Tong, D. Q., Yang, K., Lee, P., Baker, B., Crawford, A., Luke, W., Stein, A., Campbell, P. C., and Ring, A.: Air quality impacts of the 2018 Mt. Kilauea Volcano eruption in Hawaii: A regional chemical transport model study with satellite-constrained emissions, *Atmos. Environ.*, 237, 117648, <https://doi.org/10.1016/j.atmosenv.2020.117648>, 2020.
- Terraglio, F. P. and Manganelli, R. M.: The absorption of atmospheric sulfur dioxide by water solutions, *Journal of the Air Pollution Control Association*, 17, 403–406, 1967.
- Tortini, R., van Manen, S., Parkes, B., and Carn, S.: The impact of persistent volcanic degassing on vegetation: A case study at Turrialba volcano, Costa Rica, *Int. J. Appl. Earth Obs.*, 59, 92–103, 2017.
- Tzortziou, M., Herman, J. R., Cede, A., Loughner, C. P., Abuhassan, N., and Naik, S.: Spatial and temporal variability of ozone and nitrogen dioxide over a major urban estuarine ecosystem, *J. Atmos. Chem.*, 72, 287–309, 2015.
- Tzortziou, M., Parker, O., Lamb, B., Herman, J. R., Lamsal, L., Stauffer, R., and Abuhassan, N.: Atmospheric Trace Gas (NO<sub>2</sub> and O<sub>3</sub>) variability in South Korean coastal waters, and implications for remote sensing of coastal ocean color dynamics, *Remote Sensing*, 10, 1587, <https://doi.org/10.3390/rs10101587>, 2018.
- Xi, X., Johnson, M. S., Jeong, S., Fladeland, M., Pieri, D., Diaz, J. A., and Bland, G. L.: Constraining the sulfur dioxide degassing flux from Turrialba volcano, Costa Rica using unmanned aerial system measurements, *J. Volcanol. Geoth. Res.*, 325, 110–118, 2016.
- Zhang, Q., Tie, X., Lin, W., Cao, J., Quan, J., Ran, L., and Xu, W.: Variability of SO<sub>2</sub> in an intensive fog in North China Plain: Evidence of high solubility of SO<sub>2</sub>, *Particuology*, 11, 41–47, 2013.
- Zhang, R., Wang, G., Guo, S., Zamora, M. L., Ying, Q., Lin, Y., Wang, W., Hu, M., and Wang, Y.: Formation of urban fine particulate matter, *Chem. Rev.*, 115, 3803–3855, 2015.
- Zhang, X. and Schreifels, J.: Continuous emission monitoring systems at power plants in China: Improving SO<sub>2</sub> emission measurement, *Energ. Policy*, 39, 7432–7438, 2011.